CO2 methanation using sugarcane bagasse biochar/nickel sustainable catalysts

Ahmed Gamal, Mengqi Tang, Arvind Bhakta, Youssef Snoussi, Ahmed Khalil, Khouloud Jlassi, Mohamed Chehimi, Aboubakr Abdullah Ali

CO_2 methanation using sugarcane bagasse biochar/nickel sustainable catalysts

Ahmed Gamal[1], Mengqi Tang[2], Arvind K. Bhakta[2,3], Youssef Snoussi[2], Ahmed M. Khalil[4], Khouloud Jlassi[1], Mohamed M. Chehimi[2,*], Aboubakr M. Abdullah Ali[1,*]

[1]Center for Advanced Materials, Qatar University, Doha 2713, Qatar
[2]Université Paris Cité, CNRS (UMR 7086), ITODYS, F-75013 Paris, France
[3]Department of Chemistry, St. Joseph's College (Autonomous), 560027 Bangalore, India
[4]Photochemistry Department, National Research Centre, Dokki, Giza, 12622, Egypt

Abstract

Carbon dioxide hydrogenation to methane is one of the promising gas phase reactions due to the well-established natural gas infrastructures and CO_2 amounts consumed as reactants. This process supports in CO_2 mitigation, providing solutions to global warming. Using the eco-friendly sugarcane bagasse (SCB) as biochar-based catalysts, which are environmentally friendly, has not been reported for thermal catalytic CO_2 methanation. Thus, SCB biochar loaded with nickel nanocatalysts were prepared through pyrolysis, including different metal nitrate loadings on sugarcane bagasse powder ($mmol_{Ni}/g_{SCBB}$). The catalytic activity increased upon elevating the nickel nitrate loading up to 0.5 $mmol_{Ni}/g_{SCB}$ and then decreased with increasing the Ni. This is attributed to the agglomeration caused by the high content of Ni. The catalyst containing 0.5 $mmol_{Ni}/g_{SCB}$ showed the highest CO_2 conversion at all operating temperatures (250-550 °C) in addition to the highest methane selectivity at 400 °C. This study paves the way for the wide utilization of the sugarcane bagasse as an alternative green and low-cost support for various metals used in the thermal catalytic reactions, not only the CO_2 methanation. Beyond this academic research, the work contributes to address the UNs' Sustainable Development Goals SDG7 and SDG13, related to "Clean and affordable energy" and "Climate Action", respectively.

Keywords:
Biochar, Catalyst, Methane, CO_2, Hydrogenation, *Saccharum officinarum.*

***Correspondence:** mohamed.chehimi@cnrs.fr (MMC) and bakr@qu.edu.qa

1. Introduction

Many industrial and environmental applications are dedicated to reducing carbon dioxide (CO_2) in the atmosphere.[1] This crucial process may contribute to solving the global warming issue. CO_2 hydrogenation to methane (equation 1) or to methanol (equation 2) are promising applications for the utilization of CO_2 and accordingly CO_2 mitigation.[2] However, CO_2 hydrogenation to methanol requires specific operating conditions, such as high operating temperatures and applying high pressure.[3] On the other hand, the CO_2 methanation is simpler compared to the methanol production path, as it does not need relatively high operating temperature and can be carried out at the atmospheric pressure.

$$CO_2 + 4H_2 \rightarrow CH_4 + 2H_2O \qquad \Delta H_{298K} = -165 \text{ kJ/mol} \qquad \text{Eqn. 1}$$

$$CO_2 + 3H_2 \rightleftharpoons CH_3OH + H_2O \qquad \Delta H_{298K} = -49.5 \text{ kJ/mol} \qquad \text{Eqn. 2}$$

In addition, both noble and transition metal-based catalysts are used with different supports such as silica, titania, and alumina as catalysts for CO_2 methanation.[4] The noble metal-based catalysts are favored for their high gas conversion advantages.[5] However, their high cost and scarcity are critical fences preventing their large-scale application. Oppositely, nickel with its catalytic properties can replace the noble metals, particularly in chemical reductive processes.[6-8] A current approach for the development of more sustainable catalysis is the use of metals with high crustal abundance, which are often referred to as base metals. The first-row transition metals, including titanium, vanadium, chromium, manganese, iron, cobalt, nickel, and copper,

represent base metals that offer additional advantages such as low cost and global availability.[9]

A few studies reported on the immobilization of nickel onto biochar for catalyzing CO_2 methanation reaction.[10, 11] Biochar is a porous carbon material obtained from the pyrolysis of the biomass.[12] Slow pyrolysis is the preferred process for the conversion of biomass, such as agrowastes into solid biochar.[13] Slow pyrolysis at moderate temperatures (400-500 °C) ensures obtaining reasonable yield (25-40 %) with porous structure.[14] There are unlimited lignocellulosic wastes that could be converted into biochar. Agrowastes such as rice husk, sugarcane bagasse, olive pit, and many dry fruit shells are subject of numerous conversions to biochar and valorization into useful catalytic materials and electrode materials.[14, 15] Particularly, the sugarcane bagasse which constitutes ~ 26% of the sugarcane production with 700 million tons yearly produced throughout the world, has gained a particular interest, and its abundance has motivated the study of its thermochemical conversion into carbonaceous materials.[16-19] For the design of biochar supported catalysts, the pyrolysis of sugarcane bagasse can provide a porous biochar with high surface area [20]. Accordingly, it is able to improve the metal dispersion and enhance the maximum exposure of the active sites, resulting in high catalytic activity.[21] Sugarcane bagasse biochar (SCBB) could be modified with different metals for catalyzing advanced oxidation processes [14, 20, 22] as well as numerous organic chemical reactions.[23] Despite the use of SCBB composites in numerous chemical processes, it has not been considered

so far as supports in thermal catalytic gas phase reactions. This is what has motivated us to achieve this work.

Herein, we prepared the sugarcane bagasse biochar as a support for nickel to explore its catalytic activity in CO_2 methanation. Moreover, the effect of Ni loading was investigated by preparing different catalysts with different Ni contents, by simply changing the wet impregnation rate of the biomass with nickel nitrate. The composite catalyst was prepared through impregnating 0.5 mmol/g (0.5 mmol nickel per 1 g SCBB) presented the highest catalytic activity at all operating temperatures in addition to the highest methane selectivity at 400 °C. This work may pave the way for exploiting the sugarcane bagasse as a green and low-cost support for various metals used in the thermal catalytic reactions not only for the application of CO_2 methanation.

2. Methodology

2.1. Experimental Setup

The catalytic tests for CO_2 methanation were carried out in a fixed bed reactor at atmospheric pressure and at operating temperatures ranging from 250 to 500 °C, as shown in Figure 1. It depicts a schematic diagram for the experimental setup. 50 mg of the tested catalyst was placed in a quartz tube and sandwiched by two quartz wool pieces. The outlet gas pipe was connected directly to an online gas chromatograph (GC). The feed-in gases of the reaction were 40 ml/min of 40 vol.% of H_2 and 10 vol.% of CO_2 balanced in Ar (WHSV= 48000 $ml.g^{-1}.h^{-1}$). Firstly, the catalysts were activated by reduction using 40 mL/min of 10 vol.% H_2/Ar for one hour at 500 °C before starting the reaction. Then, the system was

cooled down to the room temperature and the feed gas was introduced to the catalyst while the reaction temperature was ramped up from 250 to 500 °C. Finally, the percentage of CO_2 conversion ($\%CO_2$) is calculated using equation 3, the methane selectivity ($\%CH_4$) is calculated via equation 4, and the yield of methane is calculated using equation 5. [24, 25] In addition, the turnover frequency was calculated using equation 6.[26, 27]

$$\%xCO_2 = [n(CO_{2\ In} - nCO_{2\ Out}) / CO_{2\ In}] \times 100 \qquad \text{Eqn. 3}$$

$$\%sCH_4 = nCH_{4\ Out} / nCO_{2\ converted} \qquad \text{Eqn. 4}$$

$$\%yCH_4 = nCH_{4\ Out} / nCO_{2\ In} \qquad \text{Eqn. 5}$$

$$TOF\ (s^{-1}) = [n\ CO_{2converted}\ g_{cat}^{-1} S^{-1} / S_{me}\ n\ me.g^{-1}]/time \qquad \text{Eqn.6}$$

Where, S is the second, me is the metal (Ni), S_{me} is the metallic surface area, In is the feed in, Out is the outlet amount, and n is number of moles.

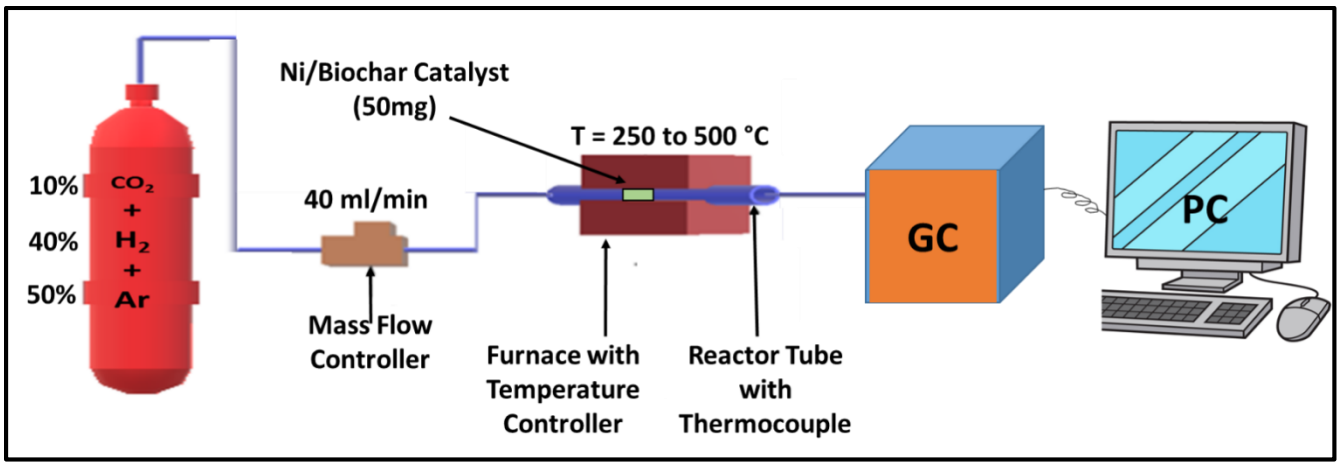

Figure 1. A schematic diagram of the experimental setup

2.2. Catalysts Synthesis

Sugarcane bagasse (SCB) was obtained from local farms in Egypt. SCB samples were dried and shredded with an electrical home appliance blender, then finely ground with coffee mill. The obtained powder was sieved and the fraction below 250 µm-sized particles was utilized as biomass feedstock to prepare biochar catalysts. Metal nitrate $Ni(NO_3)_2 \cdot 6H_2O$ (Aldrich) was used as received for impregnating the biomass. Distilled water was used to prepare nickel nitrate solutions.

Firstly, the SCB powder was added to $Ni(NO_3)_2 \cdot 6H_2O$ aqueous solutions with different molar masses. The nickel nitrate to SCB initial ratio was set at 0.1, 0.3, 0.5, 0.8 and 1.2 mmol/g, in 30 mL solution. The biomass was wet impregnated and then dried overnight at 60 °C. The catalysts were prepared as one pot synthesis by pyrolysis of the dry SCB impregnated with nickel (II) nitrate hexahydrate at 500 °C (the heating rate was 20 °C min^{-1}). Finally, the biochar catalyst was cooled to room temperature under the N_2 flow and collected. The biochar samples loaded with metal nanoparticles were denoted 0.1Ni/SCBB, 0.3Ni/SCBB, 0.5Ni/SCBB, 0.8Ni/SCBB and 1.2Ni/SCBB, respectively. In addition, another metal-free SCBB was prepared for comparison. Table 1 shows the prepared catalysts and their preparation conditions.

Table 1. Conditions of the preparation of pristine biochar and the Ni/biochar catalysts.

Sample	**SCB** (g)	**$Ni(NO_3)_2•6H_2O$** (mg)/mmol	**Distilled water** (mL)	**Before Pyrolyzed SCB+ loading material Mixture**(g)	**Biochar Mass** (g) **/Yield** (%)	**Experimental conditions**
SCBB	5.013	/	/	/	1.338/26.69	Temperature：500 °C Heating rate：10 °C/ min. Residence time：1 h Gas：N_2 atmosphere
0.1Ni/SCBB	5.000	88.04/0.1	30	5.0733	1.319/26.00	
0.3Ni/SCBB	5.000	435.2/0.3	30	5.2280	1.401/26.80	
0.5Ni/SCBB	5.000	727/0.5	30	5.6076	1.532/27. 32	
0.8Ni/SCBB	5.000	1163/0.8	30	6.1493	1.799/29.26	
1.2Ni/SCBB	5.000	1744.6/1.2	30	6.7232	1.745/25.96	

2.3. Characterization

Scanning Electron Microscopy (SEM) was used to provide high-resolution images for exploring the morphology of the prepared samples (Nova Nano SEM 450 and Quanta 200 SEM, Oregon, USA). The bulk phase and structure of the catalysts was characterized using X-ray diffraction (XRD-PANalytical-EMPYREAN, The Netherlands). Room temperature XRD measurements were performed at a scanning angle range of 5-90° and a scanning speed of 4°/min.. K Alpha^{+} X-ray photoelectron spectrometer (XPS, Thermo, East Grinstead, UK) was used for determining elemental surface composition, and main element chemical states. The elemental analyses (CHNSO) were obtained using Flash-2000 Thermo Fisher Scientific, Waltham MA, USA, to obtain the weight percentage of the carbon and nitrogen in the samples. Furthermore, Raman analyses of samples were carried out using Thermo Fisher Scientific DXR Raman Microscope, Waltham MA, USA and the thermal gravimetric analyses (TGA) were carried out in air using Pyris-6 TGA-PerkinElmer, Waltham MA, USA with a heating rate of 10 °C/min, and a temperature range of 25 to 800 °C.

3. Results and discussion

In this work we have focused on sugarcane bagasse, an abundant biomass in different countries and continents.[28] The bagasse has been first shredded and ground using home appliances (blender, then coffee mill). Sieved powder was impregnated with an aqueous solution of nickel nitrate and dried prior to pyrolysis. This thermochemical process provided Ni/Biochar powder that has been placed on quartz wool in a tubular furnace. The whole strategy, depicted in

Scheme 1, is simple, reproducible and very effective in providing biochar-based catalyst for CO_2 methanation. The rationale for using sugarcane bagasse to make biochar is the moderate to high-yield thermochemical conversion of the biomass.[14, 28] Another key issue in this work is the way to prepare biochar-immobilized nanocatalysts. There are three major methods to fabricate biochar with immobilized nanoparticles: (i) by pyrolysis under inert conditions of the biomass impregnated with metal ions ("impregnation method") [22], (ii) by in situ reduction of metal ions adsorbed on preformed biochar [29], and (iii) by mixing preformed biochar with preformed catalysts, we coin here as "micture method" [30]. These methods have been summarized and discussed in [31]. They have advantages and limitations, but if the "mixture method" should find potential industrial applications for its simplicity, we found the "impregnation method" (method (i)) to invariably yield small size nanocatalysts; this we will demonstrate below.

3.1. Characterization

XRD analyses of 0.1Ni/SCBB, 0.3Ni/SCBB, 0.5Ni/SCBB, 0.8Ni/SCBB, and 1.2Ni/SCBB confirmed the successful impregnation of Ni into the SCBB (Figure 2a). In addition, the XRD pattern indicated the existence of the metallic phase of Ni in all Ni-loaded samples, which is the active phase in the CO_2 methanation reactions.[32, 33] The Ni peaks were observed at 44.5°, 51.8° and 76.5°, which represent the crystal faces [111], [200], and [220], respectively, of the metallic Ni.[34, 35]. In addition, the XRD showed a broad peak around 23° in all samples, indicating the presence of amorphous carbon, which is

corresponding to the carbon [002].[36] The FTIR analyses of all samples showed a small broad peak at ~1100 cm^{-1}. It might be an indication for the presence of C–O–C bonds[37] in addition to other peaks observed at 1559 and 1650 cm^{-1}, which are attributed to the C–C and C=C bonds,[37] respectively, as shown in Figure 2b. The thermogravimetric analysis (TGA), carried out at air environment, showed that the metal-free SCB and the Ni/SCB catalysts have a stable thermal behavior up to ~335 °C in air, and then a slight weight loss occurred until 350 °C. The sharp decomposition started after 350 °C. The complete decomposition of all samples happened around 450 °C, which indicates the complete oxidation of carbon to carbon dioxide. In addition, the Ni/SCB catalysts were not completely decomposed and small amounts were existed even up to 800 °C. This behavior is attributed to the existence of Ni in those catalysts indicating the increasing boosting trend of metal loading (Figure 2c).

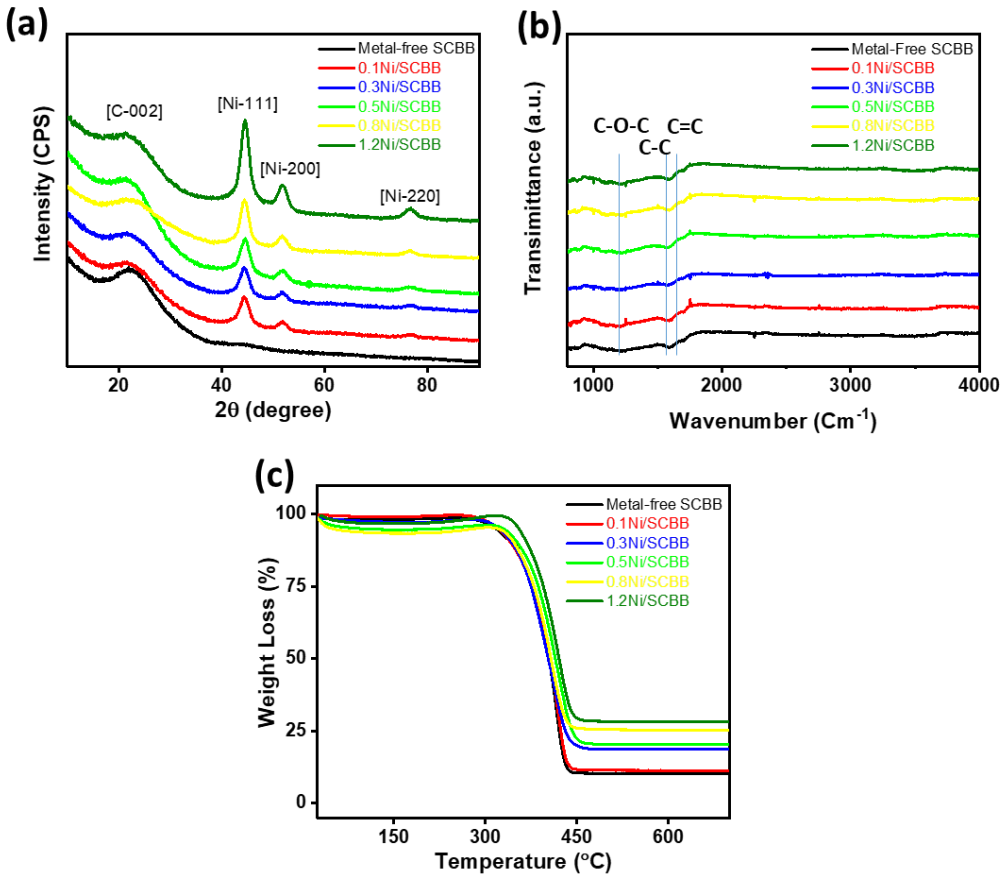

Figure 2. (a) XRD patterns, (b) FTIR spectra, and (c) thermal gravimetric analysis of SCBB and Ni/SCBB composites.

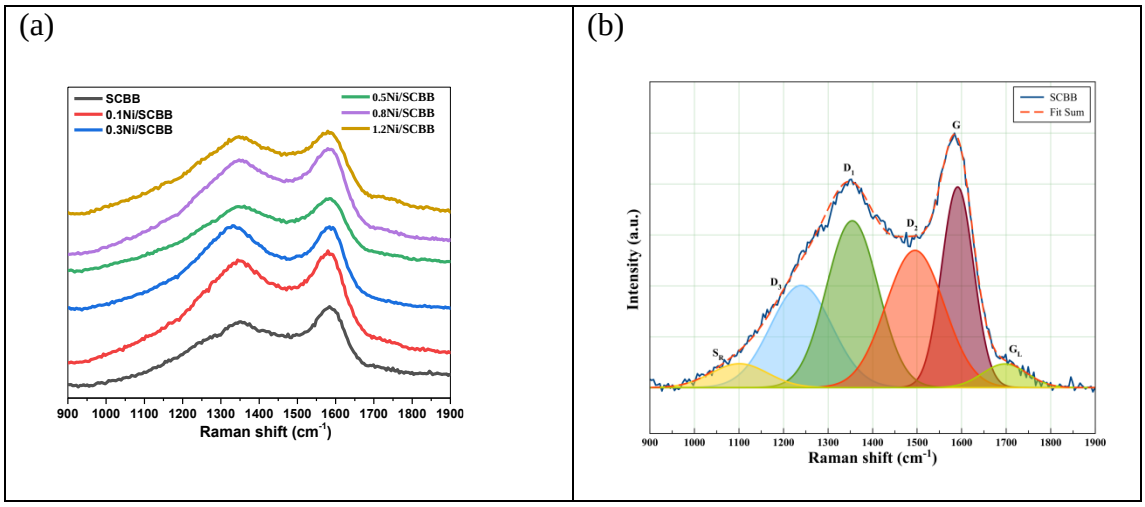

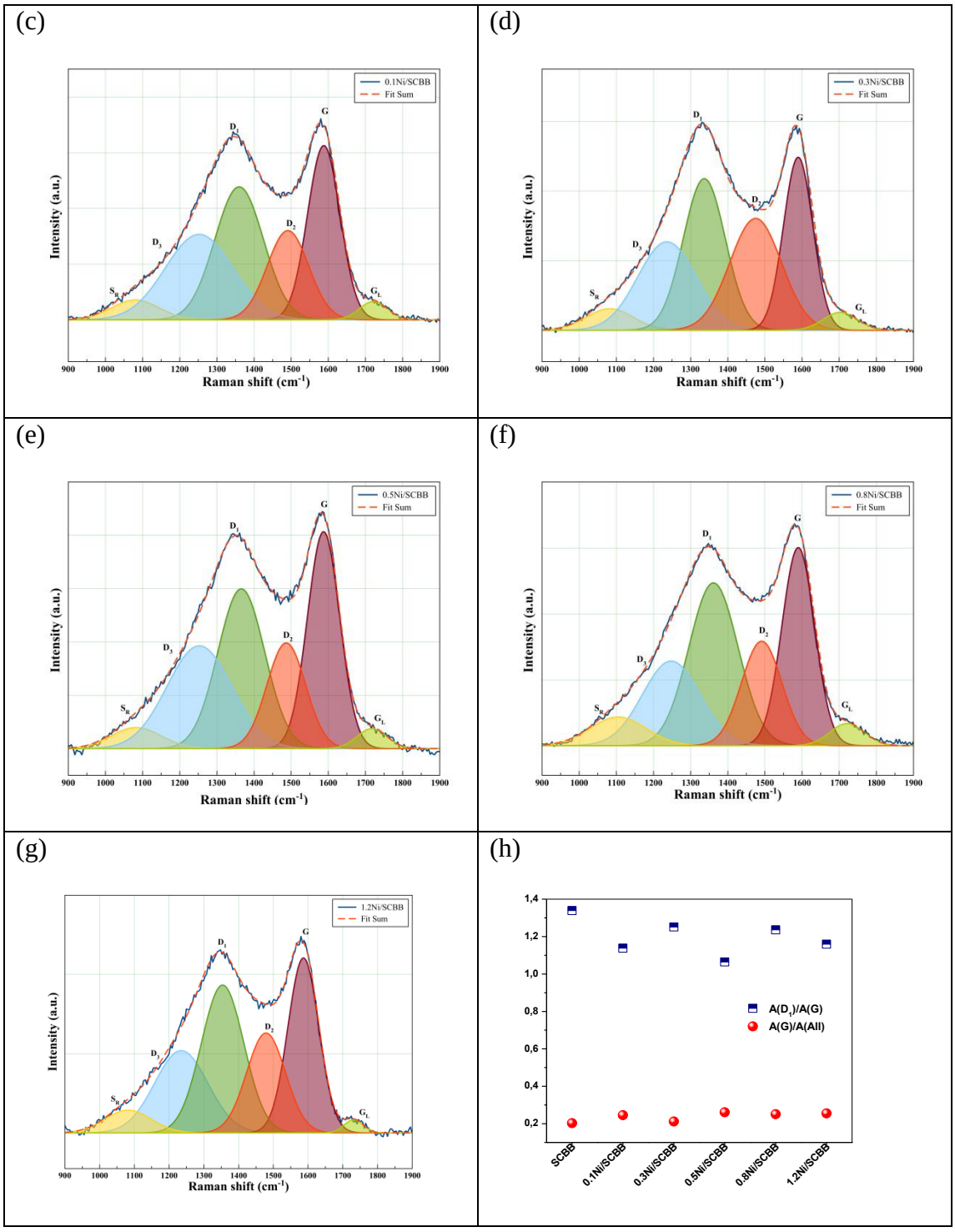

Figure 3. Raman spectra of bare SCBB and Ni/SCBB composite biochar samples: stacked spectra of pristine and Ni-modified biochar (a), curve fitted Raman spectra (b-g), and band area ratio of $A(D_1)/A(G)$ and A(G)/A(All) obtained from peak fitting (h).

The Raman spectra analysis of the investigated SCBB and Ni/SCBB samples are depicted in Figure 3. The raw spectra are stacked in Figure 3a. The samples exhibited D band at~ 1345 cm^{-1} and G band at~1580 cm^{-1}, confirming the existence of the amorphous and graphitic phases of carbon. Peak fitting the spectra permits the identification of six distinct absorption bands. A very weak S_R band (~1095 cm^{-1}) is commonly attributed to C-H within aromatic rings.[38] Notably, in the case of bituminous coal and coke, a single band within the 1200–1240 cm^{-1} range, referred to as D_3 or S band, is commonly originated from carbon structures enriched in sp^3 or sp^3-sp^2 configurations, as well as C-H groups located on aliphatic chains or aromatic rings.[39-41] The main defect band D_1 band (~1360 cm^{-1}) signifies the presence of in-plane defects or heteroatoms, correlating to the breathing mode of sp atoms within aromatic rings.[42, 43] The D_2 band centred at ~1465 cm^{-1}, also known as V_L, is assigned to aromatic rings, and amorphous carbon structures.[38] In relation to the absorption bands, the graphitic band (G band) appears at 1600 cm^{-1}, attributed to the graphitic structures.[44] Another weak G_L band (~1700 cm^{-1}) is associated with the carbonyl group of biochar catalyst.[45] The peak area ratio calculation, for relevant biochar materials, was carried out by fitting with a Gaussian function, allowing for the calculation of the $A(D_1)/A(G)$ ratio and A(G)/A(All) ratio as shown in Figure 3h. After wet impregnation with nickel, the $A(D_1)/A(G)$ ratio of all the composite materials is lower than that of pure biochar (estimated to be 1.34). It indicates a decrease in the number of defects in biochar and an increase in the uniformity of the carbonaceous structure.[44, 45] The

A(G)/A(All) ratio of different samples can be considered as an indicator of the degree of carbon order.[46] The A(G)/A(All) ratios of the Ni/SCBB materials are higher than that of pure biochar SCBB, implying that the graphitic structure is favoured in the composite metal nanoparticles.[46] Therefore, the loading of Ni nanoparticles on the biochar induces graphitization of the composite. Besides, the CHNSO analysis confirmed the carbon content of all samples, which matches with the metal loadings as the carbon decreased with increasing the Ni amount as shown in Table 2. Small amounts of hydrogen and nitrogen were detected in all samples, which might be attributed to the non-complete decomposition of the organic compounds of the biochar. Moreover, a slight decrease in the hydrogen concentration was observed with increasing the Ni content.

Table 2. The CHNSO analysis of the as-synthesized samples

Sample	C (wt.%)	H (wt.%)	N (wt.%)
Metal-free SCBB	95.61	3.23	0.94
0.1Ni/SCBB	90.47	2.93	1.13
0.3Ni/SCBB	85.33	2.76	1.16
0.5Ni/SCBB	81.10	2.66	1.18
0.8Ni/SCBB	75.92	2.47	1.51
1.2Ni/SCBB	66.19	2.19	1.64

The SEM images showed ordered honeycomb-like structures with hexagonal arrays of pores in all samples (Figure 4a-d). They offered a high porous surface area that can provide the maximum exposure of the active sites, leading to high catalytic performance.[21] In addition, Figure 4e-f shows a zoom on the porosity of the 0.5Ni/SCBB, and particularly the fishing net structure of the biochar reported by Tang et al.[22]. The elemental mapping of 0.1Ni/SCBB, 0.3Ni/SCBB, 0.5Ni/SCBB, and 1.2Ni/SCBB are shown in Figure S1. The elemental mapping of 0.1Ni/SCBB, 0.3Ni/SCBB, 0.5Ni/SCBB showed a well metal distribution, fitting well with the surface morphology of the biochar. At high metal loading, the elemental mapping of 0.8Ni/SCBB and 1.2Ni/SCBB showed high concentration of Ni with some agglomeration, as shown in the circled spots in Figure 4g-h. As will be discussed below, such an agglomeration does not favor high catalytic performances.

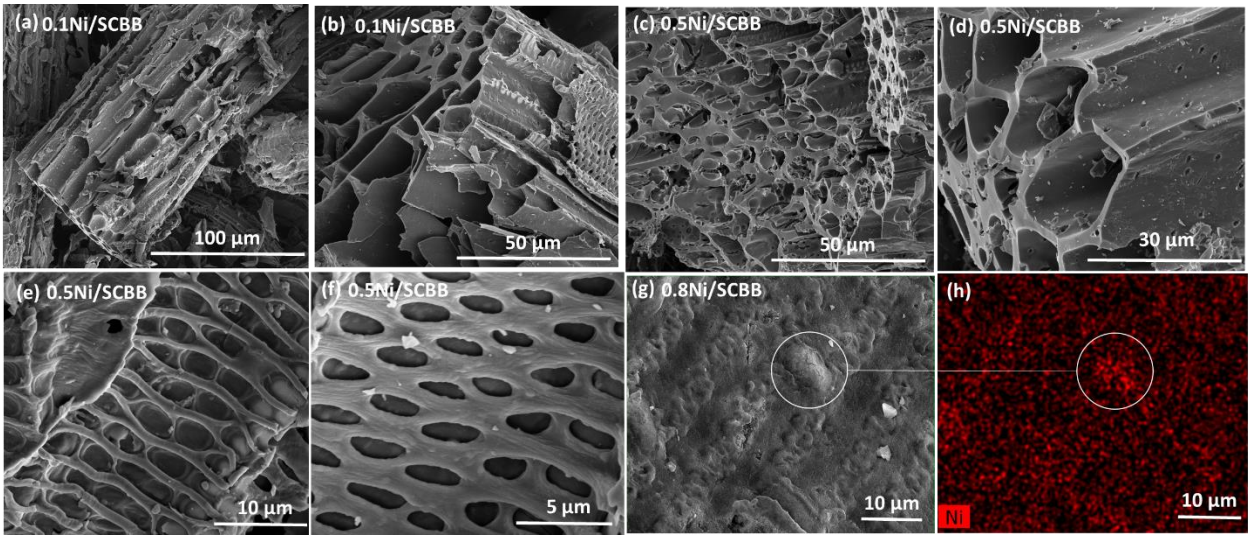

Figure 4. (a-g) SEM images of different catalysts, and (h) nickel elemental mapping of 0.8Ni/SCBB.

The EDX analyses of all catalysts confirmed the successful loading of Ni on the SCBB. Figure S2 shows the EDX analyses of 0.1Ni/SCBB, 0.3Ni/SCBB, and 0.8Ni/SCBB, and Figure 5 displays EDX spectra for SCBB (Figure 5a), 0.5Ni/SCBB (Figure 5b), and 1.2Ni/SCBB (Figure 5c). The relative peak intensity of nickel increases upon nickel nitrate impregnation of the biomass. Figure 5d depicts a plot of Ni/C atomic ratio determined by EDX versus the nickel salt impregnation rate. The plot is not quite linear; instead it shows selected materials with very close values to the calculated values, as shown in Figure 5d. Moreover, the TEM images of 0.5Ni/SCBB confirmed the excellent distribution and dispersion of Ni nanoparticles, as shown in Figure 6a and indicated the small particle size, as seen in Figure 6b, resulting in higher catalytic activity. In addition, the calculated mean size of Ni nanoparticle was ~3.8 nm as shown for 0.5Ni/SCBB (Figure 6c). On the other hand, the TEM images of 0.8Ni/SCBB showed an indication for increased population of nanoparticles, and possibly agglomeration (Figure 6d,e), resulting in less catalytic activity. In addition, the calculated average size of Ni nanoparticles of 0.8Ni/SCBB was ~5.2 nm, which is bigger than 0.5Ni/SCBB as seen in Figure 6e-f.

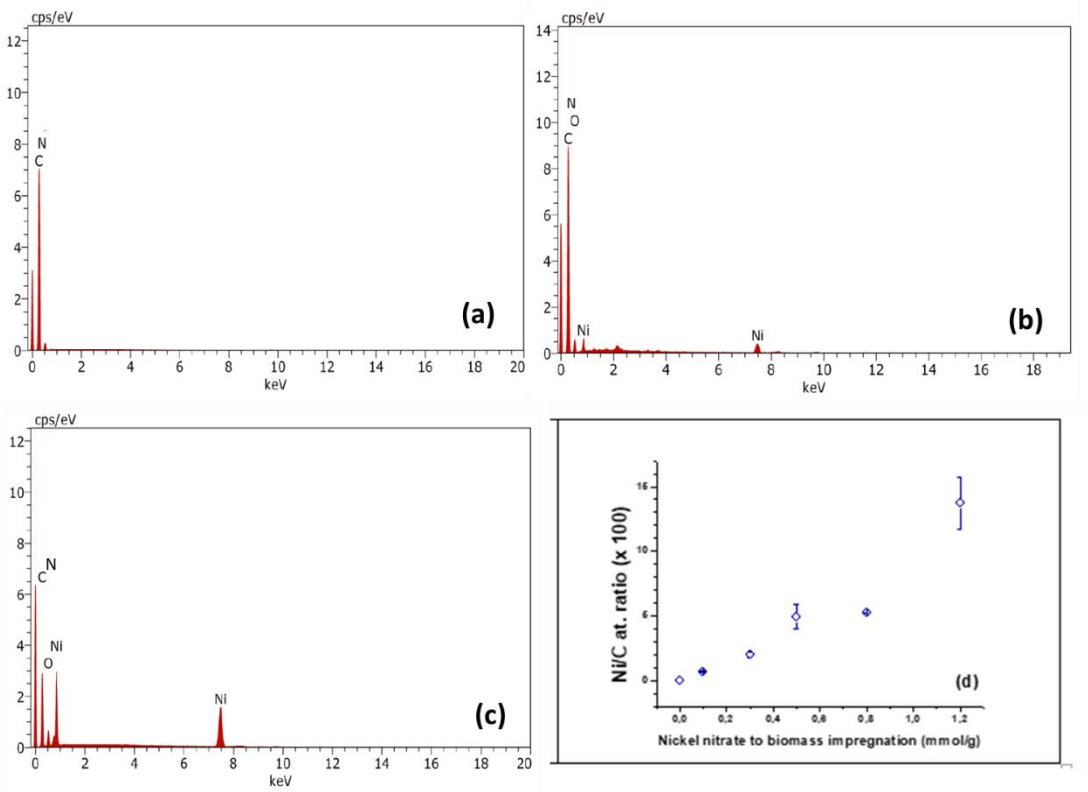

Figure 5. EDX analysis of biochar materials. EDX spectra of SCBB (a), 0.5Ni/SCBB (b), and 1.2Ni/SCBB (c). EDX-determined Ni/C atomic ratio is plotted versus the nickel impregnation of biomass (d).

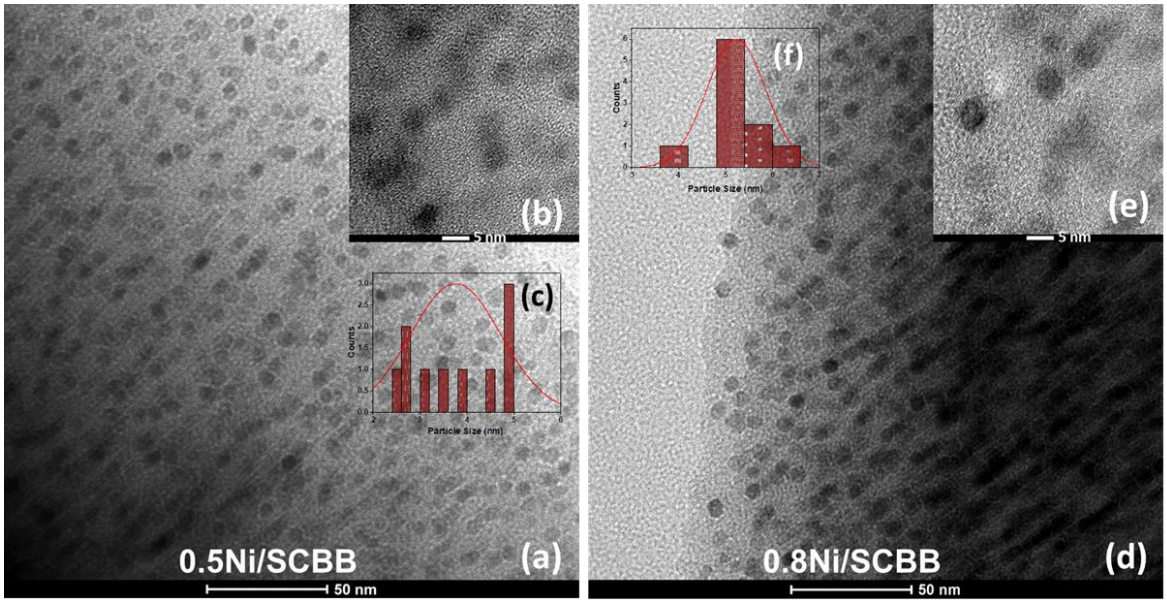

Figure 6. TEM images of 0.5Ni/SCBB (a,b) and 0.8Ni/SCBB (d,e), at two different magnifications. Nickel nanoparticle size distributions are shown in insets for 0.5Ni/SCBB (c), and 0.8Ni/SCBB (f).

The BET surface area measurements showed high surface area for all samples, which is attributed to the biochar structures. The trend of augmenting the surface area was synchronizing with the increasing of Ni loading, as shown in Table 3. It is worthy noted that the metal-free SCBB showed the lowest surface area (198 m^2/g) and 0.5Ni/SCB presented the highest surface area (620 m^2/g). It might be attributed to the high concentrations of Ni that excavate the surface creating wider pores, as indicated by the pore volume. The metal-free sample offered only 0.16 cc/g, while 0.5Ni/SCBB displayed 0.3 cc/g. Moreover, 0.8Ni/SCBB and 1.2Ni/SCBB showed less surface area than 0.5Ni/SCBB; 552 and 543 m^2/g, respectively, which might be attributed to the agglomerated Ni nanoparticles in those two catalysts, as earlier discussed.

Table 3. BET Surface area measurements and BJH pore volume measurements

Sample	**BET Surface Area (m^2/g)**	**BJH Pore Volume (cc/g)**
Metal-free SCBB	198	0.16
0.1Ni/SCBB	448	0.30
0.3Ni/SCBB	454	0.30
0.5Ni/SCBB	620	0.30
0.8Ni/SCBB	552	0.30
1.2Ni/SCBB	543	0.30

XPS was used in order to investigate the outermost surface chemical composition of the pristine and nickel-loaded biochar. Figure 7a displays all main XP spectra and data processing results. Figure 7a displays selected survey regions, covering the wet impregnation of the biomass and its effect on the final composition of the biochar. A stepwise increase in the relative peak intensity of nickel can be noted. Therefore, it testifies a control over the nanocatalyst loading by the wet impregnation method. Figure 7b plots Ni/C atomic ratio versus the initial nickel nitrate impregnation rate and confirms the monotonous increase in nickel loading, however, for an initial impregnation of 1.2 mmol metal per gram of SCB, saturation was noted. The high-resolution Ni2p region (Figure 7c) clearly exhibits two major spin-orbit doublets and satellite peaks representing the presence of both metallic nickel[47] and nickel oxide species[48, 49] resulting from air exposure of the biochar. It is worth noting that $Ni2p_{3/2}$ centred at ~852.1 eV is the core electron level peak due to the metal[47], whereas the $Ni2p_{1/2}$ centred at ~855.3 eV represents NiO[48, 49]. There is evidence for the presence of $Ni2p_{3/2}$ broad satellite peak (around 860 eV) due to nickel oxide. Figure 7d displays N1s narrow regions with pyridinic, pyrrolic and graphitic components centered at ~ 398.0, 399.6 and 401.0 eV, respectively. The pyridinic to pyrrolic ratio increases with nickel nitrate impregnation, likely due to catalytic effect of nickel in the decomposition of N-containing heterocyclic compounds.[50] Indeed, pyrrole decomposes catalytically at lower temperature than pyridine; it follows that higher loading of nickel is more effective in the decomposition of pyrrolic compared to pyridinic species.

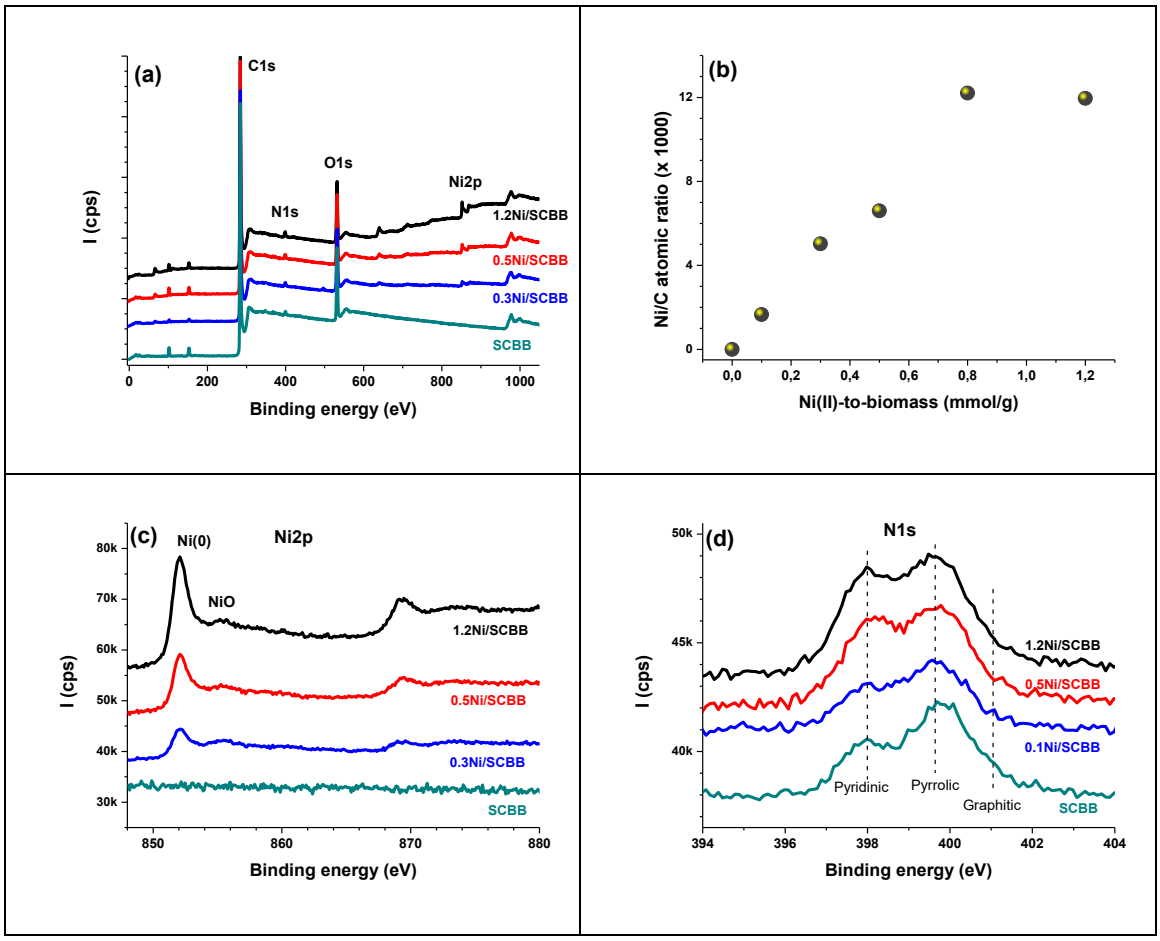

Figure 7. XPS analysis of pristine SCBB and selected Ni/SCBB samples: (a) survey regions, (b) Ni-to-initial impregnation rate plot, (c) high resolution Ni2p spectra, and (d) high resolution N1s spectra.

3.2 Catalytic Activity Tests

Firstly, the catalysts were activated in hydrogen flow at 500 °C for one hour, as a reductive atmosphere, to make sure that all Ni content included in bulk, and surface has been converted to the metallic phase, which is the active phase for the carbon dioxide hydrogenation reaction.[32, 33] The metal-free sample (SCBB) did not show any catalytic activity in all operating temperatures, while all Ni-loaded SCBB catalysts were active in the CO_2 methanation. The catalytic activity increased with increasing the Ni loadings up to 0.5mmol/g (mmol of Ni

per 1 g of SCBB). Then the catalytic activity decreased with increasing the Ni concentration, which is attributed to the agglomeration. Accordingly, 0.5Ni/SCBB showed the best catalytic performance. It could achieve the highest CO_2 conversion at all operating temperatures reaching 58% at 500 °C, as seen in Figure 8a. Moreover, it achieved the highest methane selectivity (76%) at 400 °C, as depicted in Figure 8b. Besides, 0.1Ni/SCBB, 0.3Ni/SCBB, 0.8Ni/SCBB, and 1.2Ni/SCBB were less active than 0.5Ni/SCBB regarding the CO_2 conversion and less selective to the methane production at all operating temperatures. It is also worthy noted that methane selectivity was increasing with raising the temperature until 400 °C, as an optimal temperature for methane production. The methane selectivity then decreased when the reaction temperature was raised more than 400 °C. This is ascribed to the competing reverse water gas shift reaction (RWGS)[51, 52] (equation 7), which is favored at high operating temperatures and directs the reaction to produce CO instead of CH_4, followed by the reaction of CO with the produced water to form methanol.[51, 52]

$$CO_2 + H_2 \rightleftharpoons CO + H_2O \quad \Delta H_{298K} = 41.2 \text{ kJ/mol} \qquad \text{Eqn. 7}$$

In addition, the yield of methane also followed the same trend of the methane selectivity, as it was increasing with elevating the temperature until 400 °C. Then, the yield of methane decreased when the temperature was increased due to the competed reverse water gas shift reaction (RWGS), as shown in Figure 8c. 0.5Ni/SCBB achieved 34% yield of methane at 400 °C, which is the highest yield among all tested catalysts. Figure 8d shows a comparison among all tested

catalysts at 400 °C, which was the optimal operating temperature for methane production. That comparison confirmed that the catalyst 0.5Ni/SCBB offered the highest CO_2 conversion, CH_4 selectivity, and CH_4 yield. This advantage is attributed to the well metal distribution, confirmed by the TEM analysis, and the high surface area of 0.5Ni/SCBB. For more precise assessment, turnover frequency (TOF) was determined for all catalysts, at the different operating temperatures to allow evaluating the efficiency of the catalysts. 0.5Ni/SCBB also offered the highest TOF among all catalysts, confirming that 0.5Ni/SCBB is the most active catalyst that can rapidly transform a larger number of molecules in shorter reaction time (Figure 8e), in the whole temperature range.

Furthermore, 0.5Ni/SCBB catalyst is not only the first CO_2 methanation catalyst supported on the sugarcane bagasse biochar, but also it can be located among the best reported monometallic Ni catalysts supported on biochar materials, as seen in Table 4. 0.5Ni/SCBB catalyst presented 44% carbon dioxide conversion and 76% methane selectivity at 400 °C and atmospheric pressure, which is higher than Ni/BC supported on the biochar of wheat straw[53] that showed 42 % carbon dioxide conversion and 65% methane selectivity at 450 °C and atmospheric pressure. In addition, 0.5Ni/SCBB also showed higher methane selectivity than Ni/CDC supported on cellulose-derived carbon, which displayed 67% methane selectivity at the same conditions.[54] However, Ni/CDC displayed 52% carbon dioxide conversion, which is higher than 0.5Ni/SCBB. Moreover, 0.5Ni/SCBB was superior to Ni/BC, supported on the biochar of

wheat straw that presented 45% carbon dioxide conversion and 45% methane selectivity at 500 °C.[11]

Furthermore, the other few bimetallic and trimetallic catalysts that were reported on the biochar, such as Ni-Ce and Ni-Mg-Ce presented high catalytic activity, which is attributed to the synergistic effect.[54] In addition, some researchers investigated the biochar based catalysts at higher pressure up to 10 bar and the results of the catalytic activity and especially the methane selectivity was high as seen in Table 4. However, this applied high pressure means higher cost. There are various preparation methods were reported for the rational design of the catalysts used for the CO_2 methanation, such as wet impregnation, solvothermal, chemical reduction, ammonia evaporation, and deposition precipitation. The preparation method affects the metal-support interaction and the CO_2 adsorption, and accordingly it affects the catalytic activity[55]. Table 4 shows a comparison among some promising catalysts prepared by different methods, indicating the effect of synthesis method on the catalytic activity. Further improvement of the performances of the actual Ni/biochar could be provided by incorporating carbon nitride. Such a hybridization leading to Ni/C_3N_4/biochar could potentially help boosting the already remarkable performances of the actual simple Ni/biochar, as C_3N_4/biochar is a good platform for the deposition of nanocatalysts employed in reductive processes [56, 57]. Work is in progress towards this end.

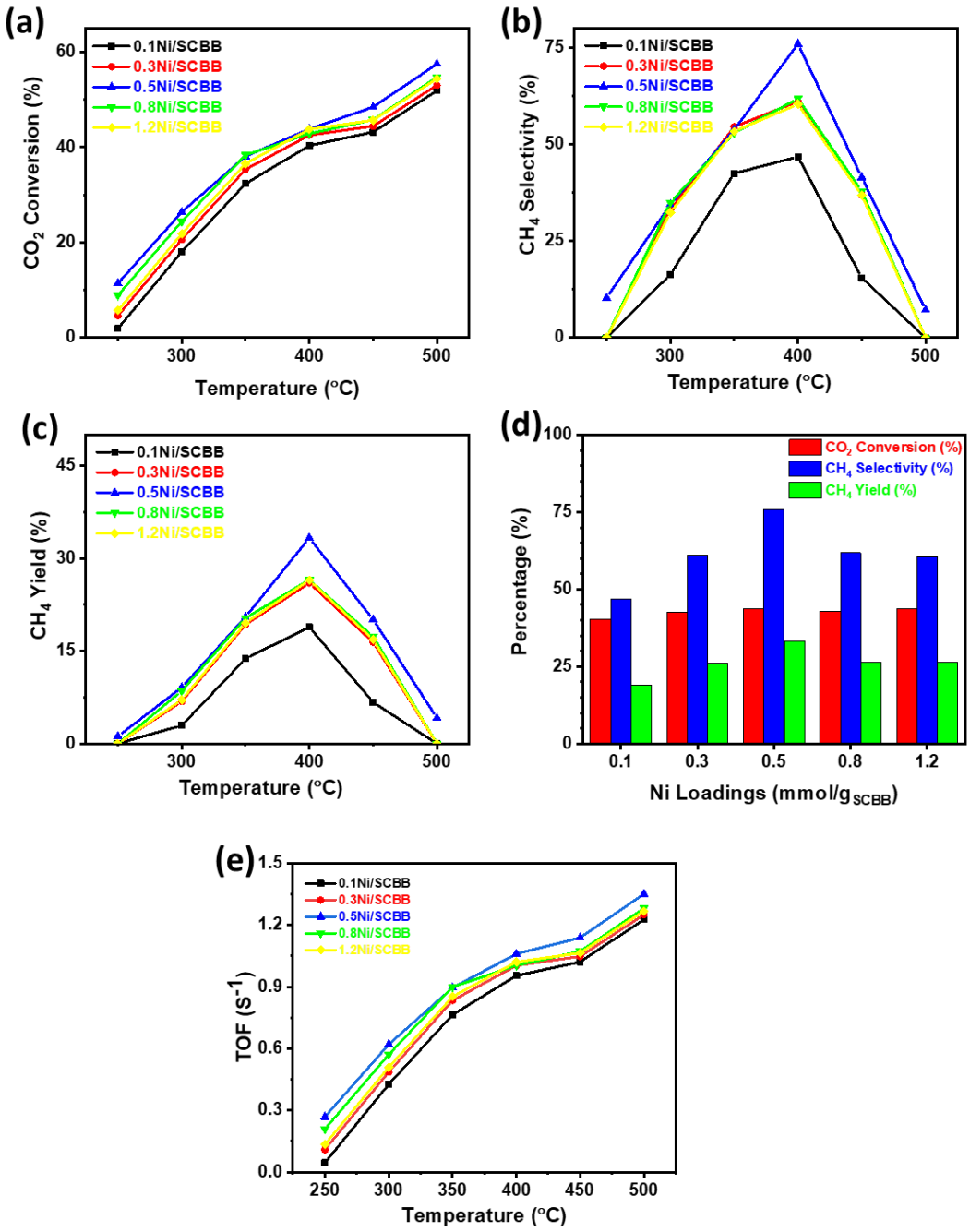

Figure 8. (a) CO_2 conversion, (b) CH_4 selectivity, CH_4 yield of all Ni/SCB catalysts.

(e) a comparison among the catalytic performance of all catalysts at 400 °C.

Table 4. A comparison among the few reported biochar-based catalysts and other reported catalysts prepared by different methods.

Catalyst	**Preparation method**	**Operation conditions**	**CO_2 conversion (%)**	**CH_4 selectivity (%)**	**Ref.**
Ni/BC	Pyrolysis	Atmospheric pressure – 450 °C	42	65	[53]
Ni-Ce/BC	Pyrolysis	Atmospheric pressure – 450 °C	65	88	[53]
Ni/CDC	Pyrolysis	Atmospheric pressure – 400 °C	52	67	[54]
Ni-Ce/CDC	Pyrolysis	Atmospheric pressure – 400 °C	78	99.9	[54]
Ni-Mg/CDC	Pyrolysis	Atmospheric pressure – 400 °C	70	97	[54]
Ni-Mg-Ce/CDC	Pyrolysis	Atmospheric pressure – 400 °C	80	99.9	[54]
Ru/ABC	Pyrolysis	10 bar – 400 °C	90	99	[5]
Ru/N-ABC	Pyrolysis	10 bar – 380 °C	93.8	99.7	[5]
Ni/ABC	Pyrolysis	10 bar – 400 °C	85	91	[10]
Ni/CeO_2	Pyrolysis	10 bar – 400 °C	92.5	90	[10]
Ni/Ce-ABC	Pyrolysis	10 bar – 400 °C	88.6	91.5	[10]
Ni/BC	Pyrolysis	10 bar – 500 °C	45	45	[11]

Ni-Ce/BC	Pyrolysis	10 bar – 400 °C	65	95	[11]
Ni/SCBB	Pyrolysis	Atmospheric pressure – 400 °C	44	76	This work
Ni/ZrO_2	Plasma Decomposition	Atmospheric pressure – 350 °C	79	76	[58]
Ni/SiO_2	Solvothermal synthesis	Atmospheric pressure – 390 °C	96	99	[59]
Ni@MOF	Wet impregnation	Atmospheric pressure – 350 °C	35	81	[60]
Ni@MOF	Solvothermal synthesis	Atmospheric pressure – 350 °C	15	45	[60]
Meso-Rh	Chemical Reduction	Atmospheric pressure – 550 °C	98	81	[61]
NP-Rh	Chemical Reduction	Atmospheric pressure – 550 °C	43	17	[61]
Ni/CeO_2-ZrO_2	Wet impregnation	Atmospheric pressure – 350 °C	51	99	[55]
Ni/CeO_2-ZrO_2	Ammonia evaporation	Atmospheric pressure – 350 °C	54	99.5	[55]
Ni/CeO_2-ZrO_2	Deposition precipitation by ammonium hydroxide	Atmospheric pressure – 350 °C	45	98.5	[55]
Ni/CeO_2-ZrO_2	Deposition precipitation using urea (DPU)	Atmospheric pressure – 350 °C	48	99	[55]

ABC: activated biochar; BC: biochar, CDC: cellulose-derived carbon, Meso: mesoporous, NP: nanoparticles.

3.3 Catalytic stability and recycling tests

A stability test was carried out to examine the durability of 0.5Ni/SCBB for 12 hours at 400 °C with weight hourly space velocity (WHSV) 48000 $ml.g^{-1}.h^{-1}$ under atmospheric pressure. 0.5Ni/SCBB presented a stable behavior for 12 h without any deactivation, as it could sustain the CO_2 conversion in the range of 42 to 44%, the CH_4 selectivity between 74 and 76, and the CH_4 yield around 33% during the whole course of the reaction, as shown in Figure 9a. Some catalysts gradually lose their catalytic activity, due to the structural changes, poisoning, overheating or the deposition of extraneous material, such as coke.[62] Thus, a recycling test was carried out using the spent catalyst 0.5Ni/SCBB, which was tested again at the same operating temperatures under the same conditions. Interestingly, the catalyst showed a robust catalytic performance, as it offered CO_2 conversion, CH_4 selectivity, and CH_4 yield similar to the fresh catalyst at all operating temperatures with a negligible fluctuation, as shown in Figure 9b-d. This high catalytic performance indicates that the catalyst is not affected by heating or by the produced water. It could sustain its structure without any changes, as shown in in Figure 10a-b, which depicts the SEM images of the spent 0.5Ni/SCBB. This is also might be attributed the reaction hydrogenation atmosphere that can keep the Ni in the metallic phase, preventing its oxidation.

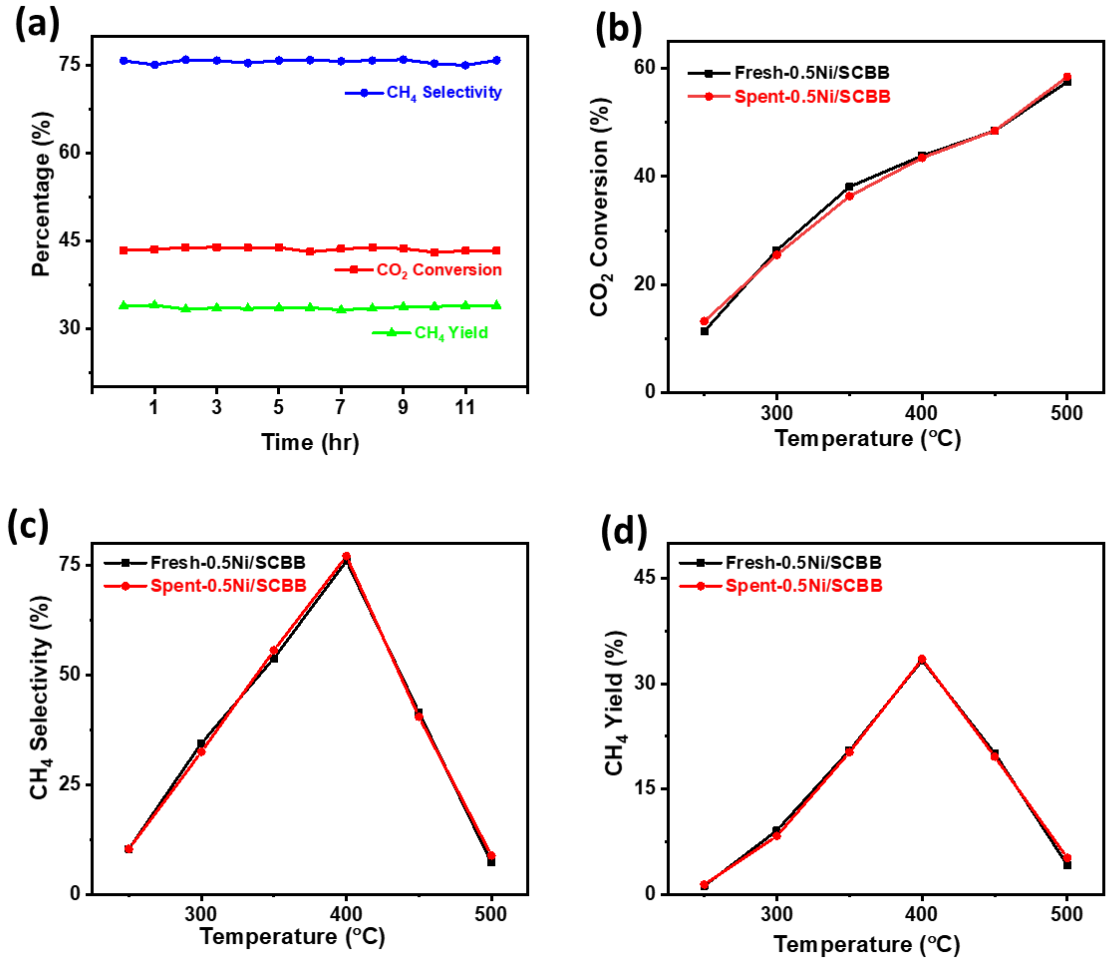

Figure 9. (a) Catalytic stability test of 0.5Ni/SCBB (b-d) CO2 Conversion, (c) CH4 selectivity, and (d) the CH4 yield of the spent 0.5Ni/SCBB catalysts.

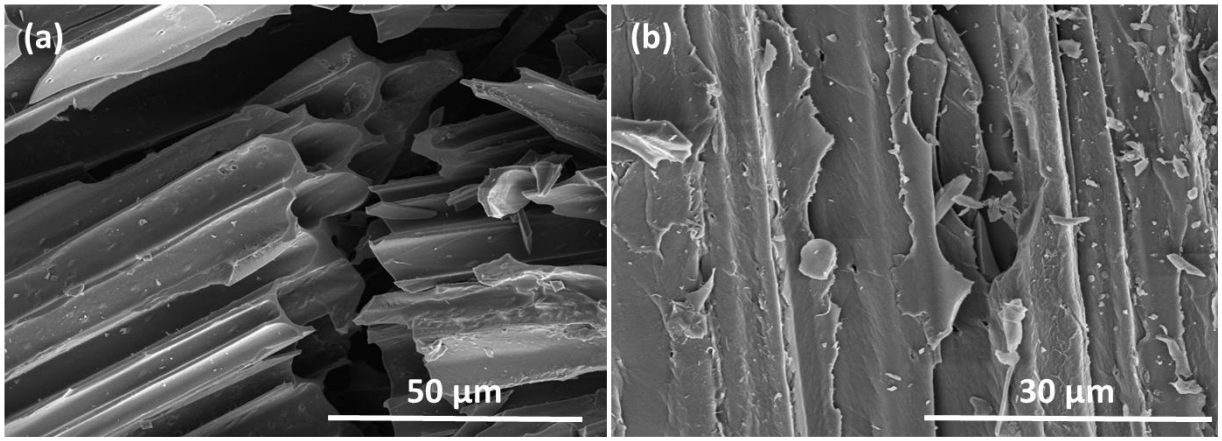

Figure 10. SEM images of the spent 0.5Ni/SCBB

4. Conclusions

Sugarcane bagasse (SCB) was modified with nickel nitrate by the wet impregnation method and pyrolyzed at 500 °C to obtain biochar with immobilized nickel nanocatalysts. The metal loading was tuned by setting the initial impregnation rate from 0.1 to 1.2 mmol nickel per 1 gram of SCB powder. All sugarcane bagasse biochar (SCBB) loaded Ni catalysts performed successfully in the CO_2 methanation, which is attributed to the high porous surface area structures provided by the SCBB. In addition, 0.5Ni/SCBB showed the highest catalytic performance among all catalysts, as it displayed the highest CO_2 conversion and the highest CH_4 selectivity at all operating temperatures. This is attributed to the well dispersion of the Ni nanoparticles, as confirmed by the SEM and TEM. The higher metal loaded catalysts; 0.8Ni/SCBB and 1.2Ni/SCBB were less active than 0.5Ni/SCBB in addition to their lower selectivity to the methane production at all operating temperatures, which is ascribed to the agglomeration caused by the high content of Ni (for example, noted by TEM for 0.8Ni/SCBB). It is also worthy noted that methane selectivity was increasing with boosting the temperature up to 400 °C, as an optimal temperature for methane production. The methane selectivity then decreased when the temperature was raised more than 400 °C, which is ascribed to the competing reverse water gas shift (RWGS). Briefly, the SCBB can be used successfully as a promising green and low-cost support for the Ni, not only in the CO_2 methanation, but also in other thermal catalytic reactions.

The protocol devised is simple, can be implemented in a friendly way, is reliable, easy to reproduce, and scalable. It addresses the UNs' SDGs 7 and 13 related to affordable energy, and climate change, respectively.

Acknowledgments

This work was supported by (i) the Qatar National Research Fund (QNRF, a member of the Qatar Foundation) through the National Priority Research Program Grant (NPRP) NPRP13S-0117-200095, and (ii) Qatar University through an International Research Collaboration Co-Fund grant, IRCC-2021-015. China Scholarship Council is acknowledged for the provision of PhD scholarship to Mengqi Tang (No 202008310221). We thank Wallonie Bruxelles International (WBI) for the provision of a grant "Bourse WBI Excellence World" (No Imputation 101386, Article Budgétaire 13 33.01.00.07). A.M.K. and M.M.C. would like to thank the French government for funding A.M.K.'s contribution through a fellowship granted by the French Embassy in Egypt (Institut Français d'Egypte).

Declaration of Interest Statement

The authors declare no conflict of interest that could have appeared to influence the presented work.

References:

[1] Shang W-L, Lv Z. Low carbon technology for carbon neutrality in sustainable cities: A survey. Sustainable Cities and Society. 2023;92:104489.
[2] Pan Y, Han X, Chang X, Zhang H, Zi X, Hao Z, et al. Enhanced Low-Temperature CO2 Methanation over Bimetallic Ni–Ru Catalysts. Industrial & Engineering Chemistry Research. 2023.
[3] Song L, Wang H, Wang S, Qu Z. Dual-site activation of H2 over Cu/ZnAl2O4 boosting CO2 hydrogenation to methanol. Applied Catalysis B: Environmental. 2023;322:122137.
[4] Riani P, Spennati E, Garcia MV, Escribano VS, Busca G, Garbarino G. Ni/Al2O3 catalysts for CO2 methanation: Effect of silica and nickel loading. International Journal of Hydrogen Energy. 2023.
[5] Wang X, Liu Y, Zhu L, Li Y, Wang K, Qiu K, et al. Biomass derived N-doped biochar as efficient catalyst supports for CO2 methanation. Journal of CO2 Utilization. 2019;34:733-41.
[6] Zhang Z, Shen C, Sun K, Jia X, Ye J, Liu C-j. Advances in Studies of Structural Effect of the Supported Ni Catalyst for CO2 Hydrogenation: From Nanoparticle to Single Atom Catalyst. Journal of Materials Chemistry A. 2022.
[7] Gac W, Zawadzki W, Rotko M, Greluk M, Słowik G, Kolb G. Effects of support composition on the performance of nickel catalysts in CO2 methanation reaction. Catalysis Today. 2020;357:468-82.
[8] Frontera P, Macario A, Ferraro M, Antonucci P. Supported catalysts for CO2 methanation: a review. Catalysts. 2017;7:59.
[9] Ludwig JR, Schindler CS. Catalyst: sustainable catalysis. Chem. 2017;2:313-6.

[10] Wang X, Yang M, Zhu X, Zhu L, Wang S. Experimental study and life cycle assessment of CO2 methanation over biochar supported catalysts. Applied Energy. 2020;280:115919.
[11] Di Stasi C, Renda S, Greco G, González B, Palma V, Manyà JJ. Wheat-straw-derived activated biochar as a renewable support of Ni-CeO2 catalysts for CO2 methanation. Sustainability. 2021;13:8939.
[12] Tripathi M, Sahu JN, Ganesan P. Effect of process parameters on production of biochar from biomass waste through pyrolysis: A review. Renewable and sustainable energy reviews. 2016;55:467-81.
[13] Pawelczyk E, Wysocka I, Gębicki J. Pyrolysis Combined with the Dry Reforming of Waste Plastics as a Potential Method for Resource Recovery—A Review of Process Parameters and Catalysts. Catalysts. 2022;12:362.
[14] Nidheesh P, Gopinath A, Ranjith N, Akre AP, Sreedharan V, Kumar MS. Potential role of biochar in advanced oxidation processes: a sustainable approach. Chemical Engineering Journal. 2021;405:126582.
[15] Lopes RP, Astruc D. Biochar as a support for nanocatalysts and other reagents: Recent advances and applications. Coordination Chemistry Reviews. 2021;426:213585.
[16] Iwuozor KO, Emenike EC, Ighalo JO, Omoarukhe FO, Omuku PE, Adeniyi AG. Review on the thermochemical conversion of sugarcane bagasse into biochar. Cleaner Materials. 2022:100162.
[17] Monteiro SN, Candido VS, Braga FO, Bolzan LT, Weber RP, Drelich JW. Sugarcane bagasse waste in composites for multilayered armor. European Polymer Journal. 2016;78:173-85.
[18] Frías M, Villar E, Savastano H. Brazilian sugar cane bagasse ashes from the cogeneration industry as active pozzolans for cement manufacture. Cement and concrete composites. 2011;33:490-6.
[19] Moretti JP, Nunes S, Sales A. Self-compacting concrete incorporating sugarcane bagasse ash. Construction and Building Materials. 2018;172:635-49.
[20] Snoussi Y, Sifaoui I, El Garah M, Khalil AM, Barroso JE, Jouini M, et al. Green, zero-waste pathway to fabricate supported nanocatalysts and anti-kinetoplastid agents from sugarcane bagasse. Waste Management. 2023;155:179-91.
[21] Zhu QL, Xia W, Akita T, Zou R, Xu Q. Metal-organic framework-derived honeycomb-like open porous nanostructures as precious-metal-free catalysts for highly efficient oxygen electroreduction. Advanced materials. 2016;28:6391-8.
[22] Tang M, Snoussi Y, Bhakta AK, El Garah M, Khalil AM, Ammar S, et al. Unusual, hierarchically structured composite of sugarcane pulp bagasse biochar loaded with Cu/Ni bimetallic nanoparticles for dye removal. Environmental Research. 2023:116232.
[23] Zhang S-Z, Cui Z-S, Zhang M, Zhang Z-H. Biochar based functional materials as heterogeneous catalysts for organic reactions. Current Opinion in Green and Sustainable Chemistry. 2022:100713.
[24] Ali S, Khader MM, Almarri MJ, Abdelmoneim AG. Ni-based nano-catalysts for the dry reforming of methane. Catalysis Today. 2020;343:26-37.
[25] Ali S, Gamal A, Khader MM. Development of highly active and coke-resilient Ni-based catalysts for low-temperature steam reformation of methane. Catalysis Communications. 2023:106605.
[26] Kozuch S, Martin JM. “Turning over” definitions in catalytic cycles. ACS Publications; 2012. p. 2787-94.
[27] Quindimil A, De-La-Torre U, Pereda-Ayo B, Davó-Quiñonero A, Bailón-García E, Lozano-Castello D, et al. Effect of metal loading on the CO2 methanation: A comparison between alumina supported Ni and Ru catalysts. Catalysis Today. 2020;356:419-32.

[28] Miranda NT, Motta IL, Maciel Filho R, Maciel MRW. Sugarcane bagasse pyrolysis: A review of operating conditions and products properties. Renewable and Sustainable Energy Reviews. 2021;149:111394.
[29] Snoussi Y, El Garah M, Khalil AM, Ammar S, Chehimi MM. Immobilization of biogenic silver-copper nanoparticles over arylated biochar from sugarcane bagasse: Method and catalytic performance. Appl Organomet Chem. 2022;36.
[30] Zarei M, Saidi K, Sheibani H. Preparation and investigation of catalytic activities of Cu-Ni nanoparticles supported on the biochar derived from pomegranate shells in the A3-coupling reactions. Biomass Conversion And Biorefinery. 2022.
[31] Geca M, Khalil AM, Tang MQ, Bhakta AK, Snoussi Y, Nowicki P, et al. Surface Treatment of Biochar-Methods, Surface Analysis and Potential Applications: A Comprehensive Review. Surfaces. 2023;6:179-213.
[32] Wierzbicki D, Debek R, Motak M, Grzybek T, Gálvez ME, Da Costa P. Novel Ni-La-hydrotalcite derived catalysts for CO2 methanation. Catalysis Communications. 2016;83:5-8.
[33] Tada S, Nagase H, Fujiwara N, Kikuchi R. What are the best active sites for CO2 methanation over Ni/CeO2? Energy & Fuels. 2021;35:5241-51.
[34] Li J, Li P, Li J, Tian Z, Yu F. Highly-dispersed Ni-NiO nanoparticles anchored on an SiO2 support for an enhanced CO methanation performance. Catalysts. 2019;9:506.
[35] Zhang S, Gai S, He F, Dai Y, Gao P, Li L, et al. Uniform Ni/SiO 2@ Au magnetic hollow microspheres: Rational design and excellent catalytic performance in 4-nitrophenol reduction. Nanoscale. 2014;6:7025-32.
[36] Lee S-M, Lee S-H, Roh J-S. Analysis of activation process of carbon black based on structural parameters obtained by XRD analysis. Crystals. 2021;11:153.
[37] Chen H, Zhang Y, Li J, Zhang P, Liu N. Preparation of pickling-reheating activated alfalfa biochar with high adsorption efficiency for p-nitrophenol: characterization, adsorption behavior, and mechanism. Environmental Science and Pollution Research. 2019;26:15300-13.
[38] Li X, Hayashi J-i, Li C-Z. FT-Raman spectroscopic study of the evolution of char structure during the pyrolysis of a Victorian brown coal. Fuel. 2006;85:1700-7.
[39] Bielowicz B, Morga R. Micro-raman spectroscopy of selected macerals of the huminite group: An example from the szczerców lignite deposit (central Poland). Energies. 2021;14:281.
[40] Sadezky A, Muckenhuber H, Grothe H, Niessner R, Pöschl U. Raman microspectroscopy of soot and related carbonaceous materials: Spectral analysis and structural information. Carbon. 2005;43:1731-42.
[41] Chabalala V, Wagner N, Potgieter-Vermaak S. Investigation into the evolution of char structure using Raman spectroscopy in conjunction with coal petrography; Part 1. Fuel Processing Technology. 2011;92:750-6.
[42] Green PD, Johnson CA, Thomas KM. Applications of laser Raman microprobe spectroscopy to the characterization of coals and cokes. Fuel. 1983;62:1013-23.
[43] Spectrum TFKJR. of Graphite. J Chem Phys. 1970;53:1126-30.
[44] Yan Q, Wan C, Liu J, Gao J, Yu F, Zhang J, et al. Iron nanoparticles in situ encapsulated in biochar-based carbon as an effective catalyst for the conversion of biomass-derived syngas to liquid hydrocarbons. Green chemistry. 2013;15:1631-40.
[45] Boraah N, Chakma S, Kaushal P. Optimum features of wood-based biochars: A characterization study. Journal of Environmental Chemical Engineering. 2023;11:109976.
[46] Zhang J, Tahmasebi A, Omoriyekomwan JE, Yu J. Production of carbon nanotubes on bio-char at low temperature via microwave-assisted CVD using Ni catalyst. Diamond and Related Materials. 2019;91:98-106.

[47] Zhang J, Chen B, Ge Y, Li Z. Efficient depolymerization of alkali lignin to monophenols using one-step synthesized Cu–Ni bimetallic catalysts inlaid in homologous biochar. Biomass and Bioenergy. 2023;175:106873.
[48] Sun B, Wang J, Chen M, Sun H, Wang X, Men Y. Boosting acetone oxidation performance over mesocrystal MxCe1-xO2 (M= Ni, Cu, Zn) solid solution within hollow spheres by tailoring transition-metal cations. Materials Chemistry and Physics. 2023;293:126925.
[49] Zhang C, Wang J, Yang S, Liang H, Men Y. Boosting total oxidation of acetone over spinel MCo2O4 (M= Co, Ni, Cu) hollow mesoporous spheres by cation-substituting effect. Journal of colloid and interface science. 2019;539:65-75.
[50] Matsuyama T, Tsubouchi N, Ohtsuka Y. Catalytic decomposition of nitrogen-containing heterocyclic compounds with highly dispersed iron nanoparticles on carbons. Journal of Molecular Catalysis A: Chemical. 2012;356:14-9.
[51] Lee WJ, Li C, Prajitno H, Yoo J, Patel J, Yang Y, et al. Recent trend in thermal catalytic low temperature CO2 methanation: A critical review. Catalysis Today. 2021;368:2-19.
[52] Stangeland K, Li H, Yu Z. CO 2 hydrogenation to methanol: the structure–activity relationships of different catalyst systems. Energy, Ecology and Environment. 2020;5:272-85.
[53] Renda S, Di Stasi C, Manyà JJ, Palma V. Biochar as support in catalytic CO2 methanation: Enhancing effect of CeO2 addition. Journal of CO2 Utilization. 2021;53:101740.
[54] Tarifa P, Megías-Sayago C, Cazaña F, González-Martín M, Latorre N, Romeo E, et al. Highly active Ce-and Mg-promoted Ni catalysts supported on cellulose-derived carbon for low-temperature CO2 methanation. Energy & Fuels. 2021;35:17212-24.
[55] Ashok J, Ang M, Kawi S. Enhanced activity of CO2 methanation over Ni/CeO2-ZrO2 catalysts: Influence of preparation methods. Catalysis Today. 2017;281:304-11.
[56] Miroliaei MR, Dadfarma A, Shahabi-Nejad M, Jalali E, Sheibani H. Biochar/g-C3N4 nano hetero-structure decorated with pt nanoparticles for diazinon photodegradation and photodeactivation under visible light. Brazilian Journal Of Chemical Engineering. 2023.
[57] Tripathi V, Reddy PL, Hande PE, Vishwakarma DS, Fartade DJ, Panchakarla LS, et al. Cobalt Nickel Bimetallic Nanocatalyst Supported on g-C3N4 for Selective Hydrogenation of α,β-Unsaturated Carbonyls and Nitroarenes. Chemcatchem. 2023;e202300460.
[58] Jia X, Zhang X, Rui N, Hu X, Liu C-j. Structural effect of Ni/ZrO2 catalyst on CO2 methanation with enhanced activity. Applied Catalysis B: Environmental. 2019;244:159-69.
[59] Ye R-P, Liao L, Reina TR, Liu J, Chevella D, Jin Y, et al. Engineering Ni/SiO2 catalysts for enhanced CO2 methanation. Fuel. 2021;285:119151.
[60] Mihet M, Grad O, Blanita G, Radu T, Lazar MD. Effective encapsulation of Ni nanoparticles in metal-organic frameworks and their application for CO2 methanation. International Journal of Hydrogen Energy. 2019;44:13383-96.
[61] Arandiyan H, Kani K, Wang Y, Jiang B, Kim J, Yoshino M, et al. Highly selective reduction of carbon dioxide to methane on novel mesoporous Rh catalysts. ACS applied materials & interfaces. 2018;10:24963-8.
[62] Gamal A, Eid K, Abdullah AM. Engineering of Pt-based nanostructures for efficient dry (CO2) reforming: Strategy and mechanism for rich-hydrogen production. International Journal of Hydrogen Energy. 2022;47:5901-28.